Supplementary Information

Fluorescence and Colorimetric Dual-mode Multienzyme Cascade Nanoplatform Based on CuNCs/FeMn-ZIF-8/PCN for Detection of Sarcosine

Yu Wu,[a,b] Chenxi Ke,[a,b] Zichen Song,[a,b] Hongda Zhu,[a,b] Huiling Guo,[a,b] Hongmei Sun[a,b] and Mingxing Liu *[a,b]

[a] Cooperative Innovation Center of Industrial Fermentation (Ministry of Education & Hubei Province), National "111" Center for Cellular Regulation and Molecular Pharmaceutics, Key Laboratory of Fermentation Engineering (Ministry of Education), Hubei University of Technology, Wuhan, 430068, People's Republic of China

[b] Hubei Key Laboratory of Industrial Microbiology, School of Biological Engineering and Food, Hubei University of Technology, Wuhan, 430068, People's Republic of China

[*] Corresponding author.

Corresponding author at: Cooperative Innovation Center of Industrial Fermentation (Ministry of Education & Hubei Province), School of Biological Engineering and Food, Hubei University of Technology, Wuhan 430068, People's Republic of China.

E-mail address: lmxing@hbut.edu.cn (M.X. Liu)

Section S1. Reagents and Materials.

Iron(II) sulfate heptahydrate ($FeSO_4•7H_2O$), Zinc nitrate hexahydrate ($Zn(NO_3)_2•6H_2O$), Copper(II) sulfate pentahydrate ($CuSO_4•5H_2O$), potassium ferricyanide(III) ($K_3[Fe(CN)_6]$), ammonium dihydrogen phosphate ($NH_4H_2PO_4$), 2-methylimidazole (2-MIM), methanol, and H_2O_2 (30 %), purchased from Sinopharm Chemical Reagent Co., Ltd (Shanghai, China). *p*-Benzoquinone, Isopropyl alcohol, Glutathione reduced, sarcosine, catalase (CAT), and quinine sulfate dihydrate were obtained from Shanghai Macklin Biochemical Co., Ltd (Shanghai, China). Manganese(II) nitrate tetrahydrate ($Mn(NO_3)_2•4H_2O$), 3,3',5,5'-tetramethylbenzidine (TMB), and peroxidase from horseradish (HRP), were from Shanghai Aladdin Biochemical Co., Ltd (China). Sarcosine oxidase (SOX) was the product of Yuanye Biotechnology Co., Ltd. (Shanghai, China). The Human Sarcosine ELISA Kit was from COIBO BIO Inc. (Shanghai, China). Ultrapure water from a water purification system (18.2 MΩ cm, Bedford Millipore, Ma, USA) was used in all experiments.

To evaluate the feasibility of the dual-mode multienzyme cascade nanoplatform, human urine samples were collected from the Hospital of the Hubei University of Technology and approved by the Ethics and Safety Committee of Scientific Research of the Hubei University of Technology.

Section S2. Apparatus.

A range of approaches were used to investigate the phase structures of samples. Specifically, powder X-ray diffraction (XRD; Bruker D8 Advance, Karlsruhe, Germany) with the 2θ range of 5°–80° was used to identify the crystal structures. The elemental distribution was studied with transmission electron microscopy (TEM) and energy dispersive spectroscopy (EDS) (Talos F200X, Thermo Fisher). The X-ray photoelectron spectra (XPS) were obtained on Versaprobel PHI 5000. UV spectroscopy between 800 and 200 nm (Lambda35 spectrophotometer, PerkinElmer), FL spectroscopy between 600 and 350 nm (RF-6000 fluorescence spectrophotometer, Shimadzu), and FT-IR spectroscopy between 400 and 4000 cm^{-1} (Nicolet 5700, Thermo) were used to describe the samples' optical properties.

Section S3. Materials preparation.

Synthesis of GSH-CuNCs. GSH-CuNCs were prepared by a slightly modified method.[1] 2 mL of 0.1 M GSH solution was mixed with 0.13 mL of the same concentration $CuSO_4 \cdot 5H_2O$ solution, which was then mixed with 1 mL of 1 M NaOH solution to increase GSH's reducing capacity. The resultant liquid was diluted to 20 mL and stirred for 8 h at 90 ℃. Before use, the resulting solution was refrigerated at 4 °C.

Preparation of PCN nanosheets. Firstly, the bulk nanomaterials of carbon nitride were prepared by the roasting method.[2] 1 g of urea was dissolved in 10 mL of ultrapure water; the solution was magnetically stirred at room temperature for 30 min, 0.2 g of ammonium dihydrogen phosphate was added to this reaction mixture, and then sonicated for 10 min. The prepared solution was spin-steamed at 60 °C to remove water and dried in a vacuum drying oven at 70 °C for 2 h. The resulting precipitate was cooled and reacted in a crucible at 550 ºC for 2 h. The solid product was ground into powder for further use to obtain bulk PCN. Next, 1 g of bulk PCN was dispersed in 20 mL of ultrapure water, sonicated for 8 h, and centrifuged at 1000 rpm for 10 min. The resulting supernatant was stirred in HCl (37 %) for 10 h, centrifuged at 8000 rpm for 10 min, washed three times with ultrapure water, and freeze-dried to obtain PCN nanosheets.

Synthesis of FeMn-ZIF-8 and SOX@FeMn-ZIF-8. To synthesize FeMn-ZIF-8, ZIF-8 was first synthesized by modification based on the reported method.[3] 100 mg $Zn(NO_3)_2 \cdot 6H_2O$ was dissolved in 5 mL methanol, and 10 mL of 22 mg/mL of 2-methylimidazole (2-MIM) methanol solution was slowly added to it, stirred at room temperature for 25 min; the mixed solution turned milky gradually. The product ZIF-8 was obtained by centrifugation at 8000 rpm for 10 min and washed three times with methanol. ZIF-8 was dispersed in 5 mL methanol, and 2 mL of $FeSO_4 \cdot 7H_2O$ solution and $Mn(NO_3)_2 \cdot 4H_2O$ solution at a concentration of 1 mg/mL were added to it, respectively. After stirring for 5 h, the mixture was centrifuged at 8000 rpm for 10 min, and the products were washed three times with methanol. The well-dispersed liquid was stirred at room temperature for 5 h, centrifuged at 8000 rpm for 10 min, washed with methanol 3 times, and freeze-dried.

To synthesize SOX@FeMn-ZIF-8, 10 mg $Zn(NO_3)_2•6H_2O$ and 1 mg SOX were dissolved in 3 mL ultrapure water and slowly added to 2 mL 5.5 mg/mL 2-MIM aqueous solution, stirred at room temperature for 25 min, centrifuged at 8000 rpm for 10 min. The precipitate was washed three times with ultrapure water, and then the product SOX@ZIF-8 was dispersed in 5 mL of ultrapure water. Then 500 μL of $FeSO_4•7H_2O$ solution and $Mn(NO_3)_2•4H_2O$ solution (1 mg/mL) were added to the mixture. The mixture was kept stirring for 5 h at room temperature and then the yellowish product was collected followed by centrifuged at 8000 rpm for 10 min, and rinsed three times with ultrapure water and freeze-dried.

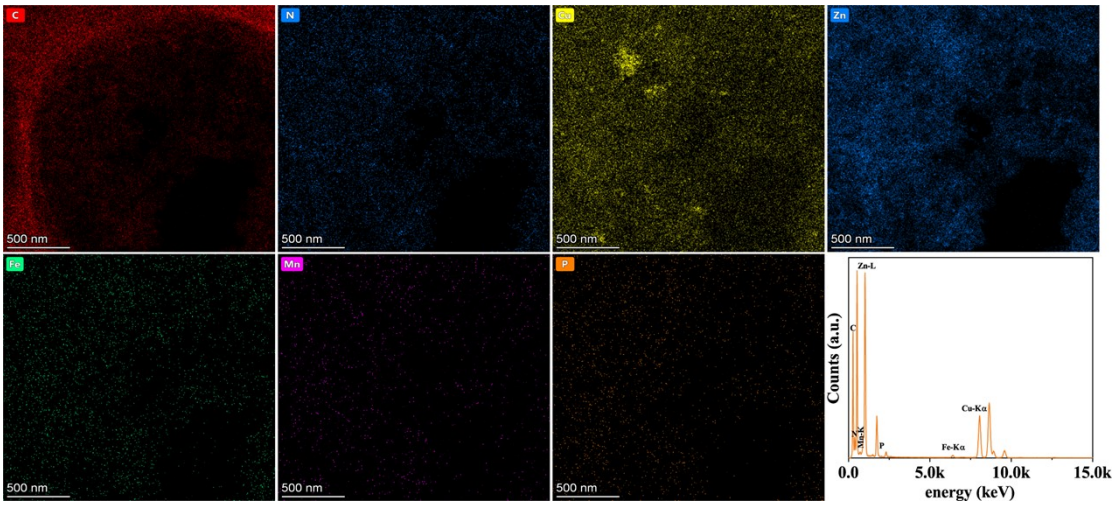

Fig. S1 Element mapping images and EDS spectra of CuNCs/FeMn-ZIF-8/PCN.

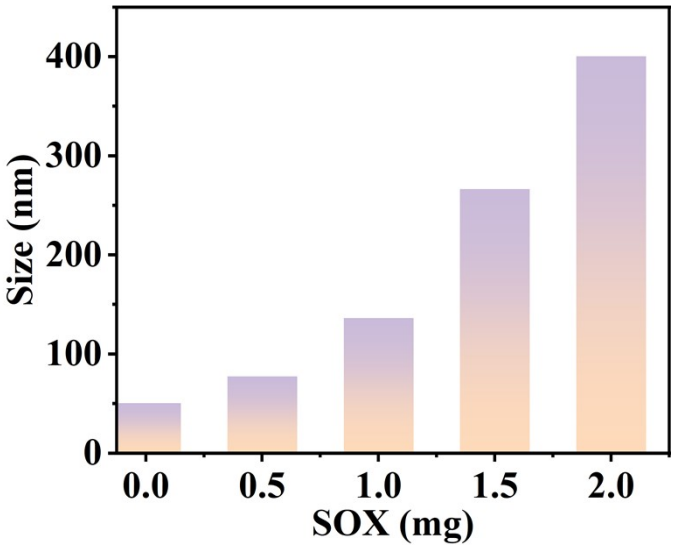

Fig. S2 Effect of SOX addition amount on SOX@FeMn-ZIF-8 particle size.

The impact of the varying amounts of SOX on the hydration particle size of FeMn-ZIF-8 has been investigated. As the addition of SOX plays a guiding role in the morphological control of FeMn-ZIF-8, influencing the crystal growth process, the hydration particle size of SOX@FeMn-ZIF-8 tends to gradually increase with an increase in the amount of added SOX, ranging from 0 mg to 2 mg.

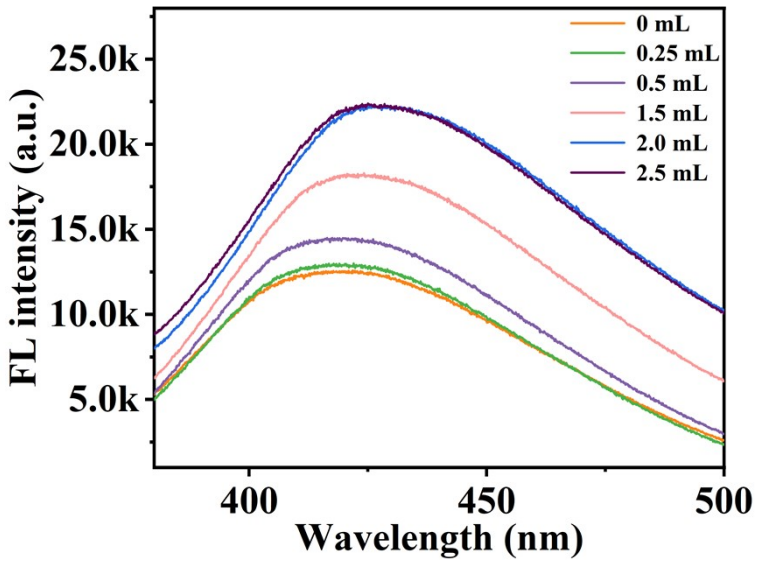

Fig. S3 Effect of CuNCs addition amount on FL intensity of CuNCs/FeMn-ZIF-8.

As shown in Fig. S3, with the increasing amount of added CuNCs, the FL intensity of CuNCs/FeMn-ZIF-8 also increases. This is attributed to the immobilization of CuNCs on FeMn-ZIF-8, restricting the vibration and rotation of the ligand GSH on CuNCs. As a result, most of the excited-state electrons return to the ground state through radiative decay rather than non-radiative decay, leading to FL intensity enhancement. Additionally, FeMn-ZIF-8 significantly reduces the quenching effect of molecules approaching CuNCs, preventing adverse solvent relaxation on the FL of CuNCs. Therefore, the FL intensity of CuNCs/FeMn-ZIF-8 is enhanced. When the added amount of CuNCs reaches 2 mL, the FL intensity of the material no longer continues to increase. This is because FeMn-ZIF-8 cannot immobilize additional CuNCs, indicating that 2 mL is the optimal amount of CuNCs to be added.

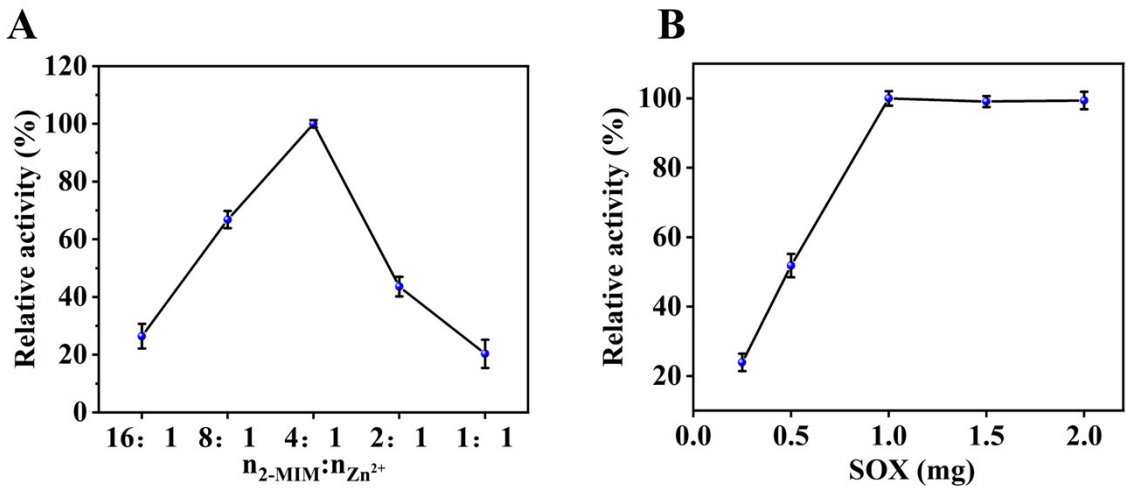

Fig. S4 The effect of the ratio of the amount of 2-MIM to Zn2+ on SOX activity; Effect of addition amount of SOX on SOX@ZIF-8 activity.

As shown in Fig. S4A, the synthesis conditions for SOX@ZIF-8 were optimized using a single-variable control method. Initially, with a fixed concentration of SOX, the ratio of 2-MIM to Zn^{2+} was varied. When the ratio of 2-MIM to Zn^{2+} was 16:1, SOX@ZIF-8 exhibited the lowest relative activity. With an increase in the concentration of 2-MIM, the activity of SOX@ZIF-8 gradually increased. However, when the ratio of 2-MIM to Zn^{2+} was 4:1, the activity of SOX@ZIF-8 was highest, followed by a decline. This phenomenon is attributed to the provision of four empty orbitals by the outer 4s and 4p orbitals of Zn^{2+}, coordinating with the four nitrogen atoms on 2-MIM to form regular ZnN_4 clusters. These clusters are connected by imidazole rings, creating a cage-like crystal structure. Excessive or insufficient 2-MIM disrupts the normal crystal growth, resulting in decreased porosity of ZIF-8.[4] Consequently, the enzyme loading capacity and enzymatic activity of SOX@ZIF-8 are reduced. The optimization results for SOX quantity indicate, as shown in Fig. S4B, that with an increase in SOX quantity, the relative activity of SOX@ZIF-8 gradually rises. When the SOX concentration reaches 1 mg, the activity of SOX@ZIF-8 is maximized, and thereafter, there is no significant improvement. This is attributed to the limited capacity of the carrier, preventing the immobilization of excess SOX.

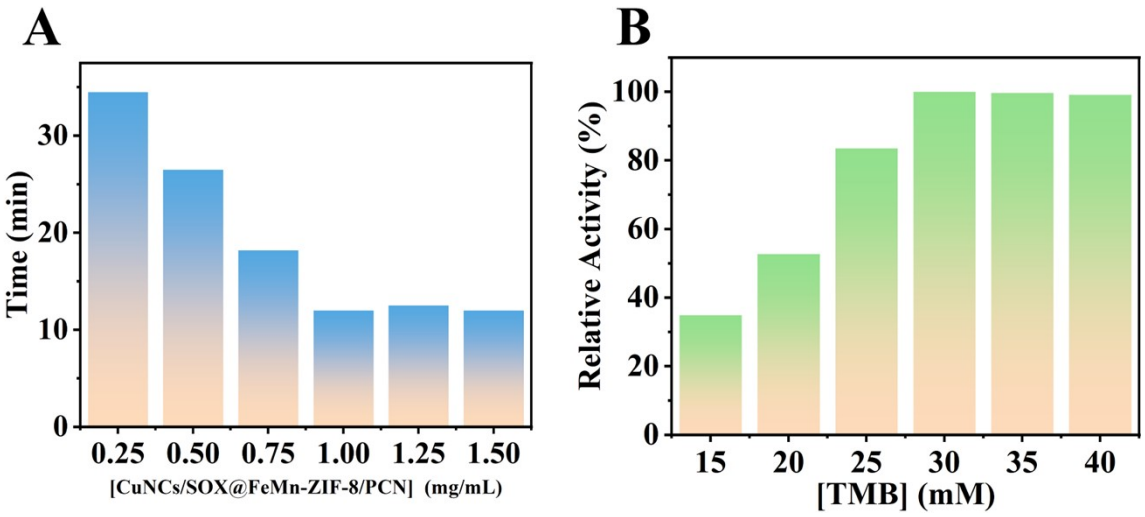

Fig. S5 (A) Effect of CuNCs/SOX@FeMn-ZIF-8/PCN concentration on the time of SA reaching equilibrium detected by FL pattern; (B) The effect of TMB concentration and color pattern on SA detection.

The impact of the concentration of CuNCs/SOX@FeMn-ZIF-8/PCN on the time to reach reaction equilibrium in the FL mode detection of SA has been discussed. As shown in Fig. S5A, with increasing concentrations, the time required for the reaction to reach equilibrium decreases. When the concentration reaches 1 mg/mL, the reaction time is minimized. Higher concentrations of the material would generate more waste, increasing experimental costs. Therefore, the optimal concentration selected is 1 mg/mL. The influence of TMB concentration on the colorimetric detection of SA is illustrated in Fig. S5B. Setting the highest absorbance value as 100%, the absorbance increases with the rising TMB concentration. When the TMB concentration reaches 30 mM, the absorbance peaks. Subsequently, further increases in TMB concentration do not lead to additional absorbance, hence 30 mM TMB is chosen as the optimal chromogenic agent.

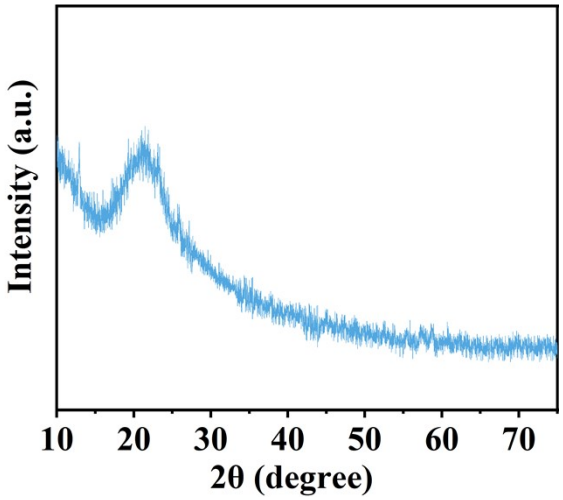

Fig. S6 The XRD patterns of CuNCs.

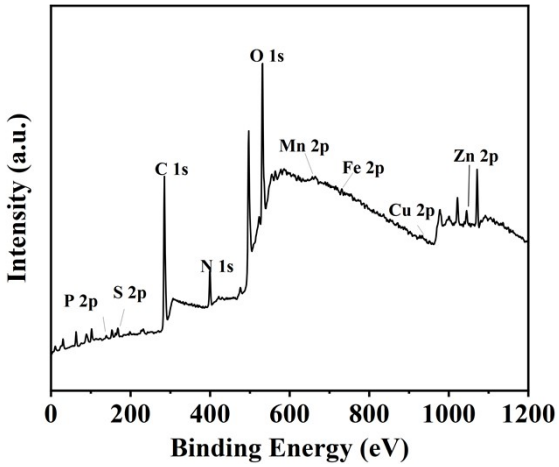

Fig. S7 XPS spectra of CuNCs/FeMn-ZIF-8/PCN.

Table S1 Related data of quantum yields of CuNCs and CuNCs/FeMn-ZIF-8/PCN

Samples	η	A	I	QYs (%)
CuNCs	1.33	0.133	1502907.5	11.17
CuNCs/FeMn-ZIF-8/PCN	1.33	0.152	4096810.6	34.81
Quinoline sulfate	1.33	0.115	8399364.3	54

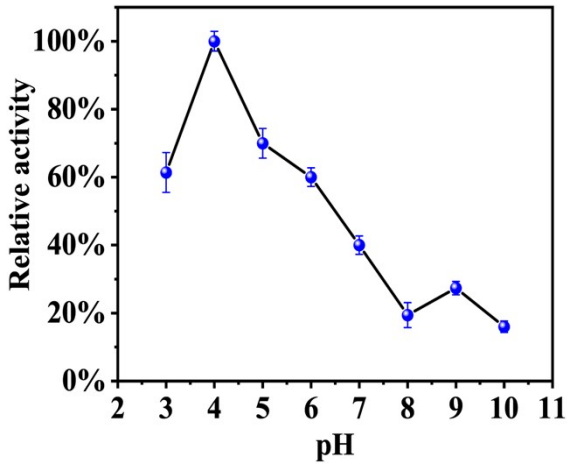

Fig. S8 Effect of pH on the enzymatic-like activity of CuNCs/FeMn-ZIF-8/PCN.

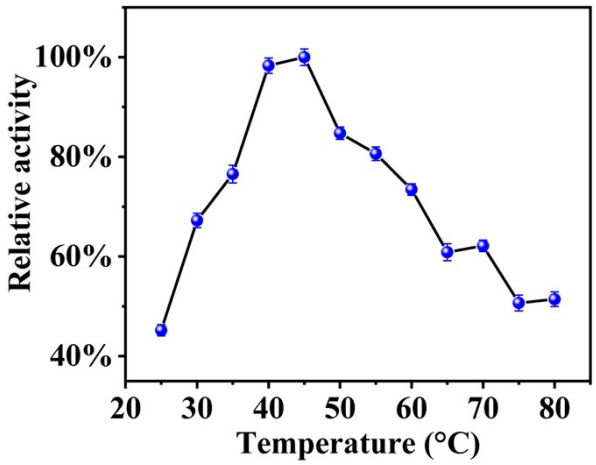

Fig. S9 Effect of temperature on the enzymatic-like activity of CuNCs/FeMn-ZIF-8/PCN.

Table S2 Comparison of enzyme kinetic parameters of different material

Enzyme	K_m (mM)		V_{max} (10^{-8} Ms^{-1})		Reference
	TMB	H_2O_2	TMB	H_2O_2	
$MgFe_2O_4$ MNPs	0.67	4.61	2.09	13.46	5
MA-Hem/Au−Ag	2.39	2.70	1.42	11.40	6
IrO_2/rGO	0.28	229.00	42.70	372.90	7
CuNCs	0.29	2.22	6.79	1.14	This work
FeMn-ZIF-8	0.38	4.05	5.88	6.02	This work
Fe-ZIF-8	0.42	3.21	6.4	5.8	This work
PCN	0.30	3.38	5.30	5.04	This work
GCN	0.83	5.24	4.62	4.14	This work
HRP	0.41	2.78	6.75	5.89	This work
CuNCs/ FeMn-ZIF-8/PCN	0.23	2.10	7.59	9.32	This work

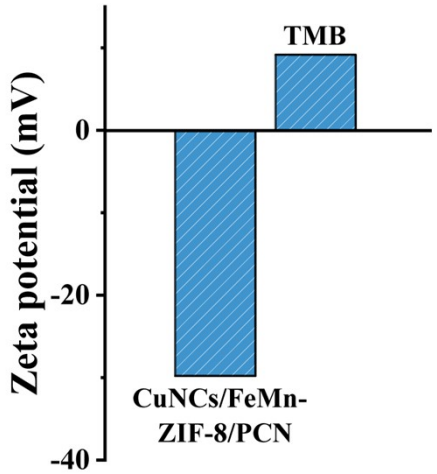

Fig. S10 Zeta potential of CuNCs/FeMn-ZIF-8/PCN and TMB.

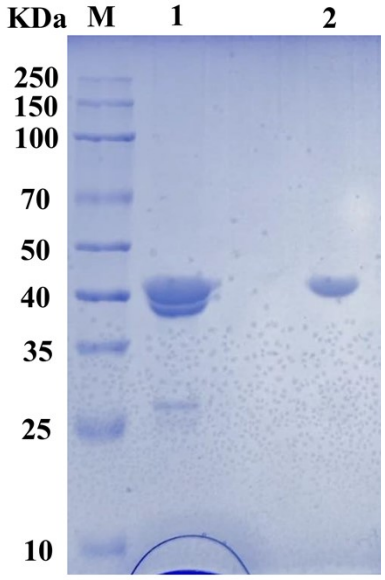

Fig. S11 SDS–PAGE gel (M: protein marker, lane 1: free SOX, lane 2: CuNCs/SOX@FeMn-ZIF-8/PCN.)

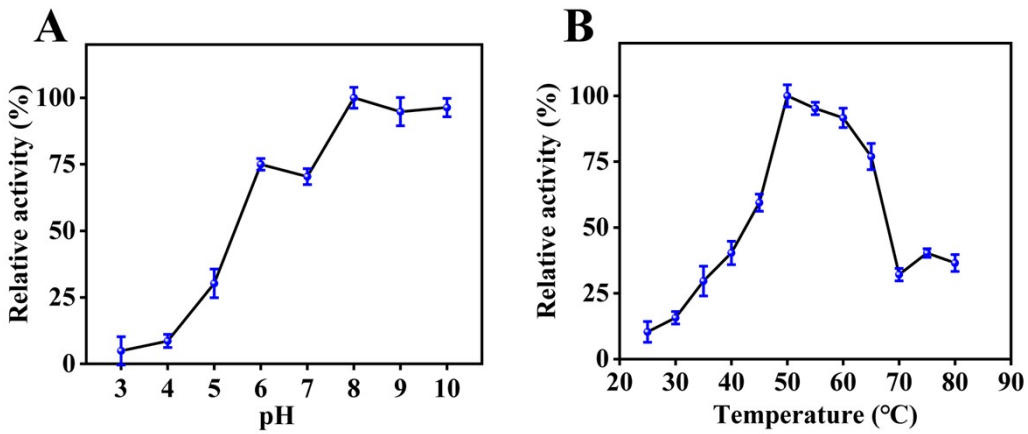

Fig. S12 Optimal pH (A) and temperature (B) for CuNCs/SOX@FeMn-ZIF-8/PCN multienzyme cascade reaction.

Table S3 Compare the method of this work with the previously reported method for detecting SA

Detection method	LOD (μM)	Linear range	Reference
Electrochemical sensor	—	5 - 30	8
FL sensor	0.36	1-80	9
Electrochemical sensor	0.8	2-70	10
Colorimetric sensor	0.6	0-10	11
Electrochemical sensor	0.5	0.5-7.5	12
Electrochemical sensor	0.43	0.5-60	13
Colorimetric sensor	15	28.6-190.5	14
FL sensor	0.17	1-20	15
Dual-mode sensor	FL (0.34) Colorimetric (0.59)	FL (1-100) Colorimetric (1-200)	This work

Table S4 Added-standard recovery results for quantification of SA in human urine samples with FL channel (n=3)

Sample	Detected Result (μM) ±SD	Added (μM)	Found (μM) ±SD	Recovery (%)	RSD (%)
1	2.84±0.09	15	17.02±0.37	95.4	2.17
		60	63.86±0.51	101.62	0.80
2	2.65±0.06	15	17.14±0.31	97.11	1.81
		60	62.49±0.49	99.74	0.78
3	2.62±0.08	15	17.72±0.43	100.57	2.43
		60	61.50±0.38	98.21	0.62
4	2.75±0.12	15	17.68±0.31	99.61	1.75
		60	64.10±0.46	102.15	0.72
5	2.39±0.11	15	17.42±0.51	100.17	2.93
		60	61.19±0.63	98.08	1.03
6	2.59±0.09	15	17.77±0.39	101.02	2.19
		60	61.07±0.72	97.57	1.18
7	2.48±0.15	15	17.98±0.32	102.86	1.78
		60	62.65±0.53	100.27	0.85
8	2.64±0.11	15	17.19±0.41	97.45	2.39
		60	64.64±0.59	103.19	0.92
9	2.25±0.11	15	17.01±0.53	98.61	3.12
		60	63.95±0.61	102.73	0.95
10	2.24±0.10	15	17.42±0.59	101.04	3.39
		60	62.43±0.64	103.52	1.03

Table S5. Added-standard recovery results for quantification of SA in human urine samples with colorimetric channel (n=3)

Sample	Detected Result (μM) ±SD	Added (μM)	Found (μM) ±SD	Recovery (%)	RSD (%)
1	2.86±0.08	15	17.51±0.52	98.04	2.97
		60	63.98±0.76	101.78	1.19
2	2.60±0.11	15	17.13±0.42	97.32	2.45
		60	62.01±0.67	99.06	1.08
3	2.54±0.11	15	17.01±0.34	96.97	2.00
		60	61.39±0.75	98.16	1.22
4	2.79±0.16	15	17.01±0.63	95.62	3.70
		60	62.13±0.64	98.95	1.03
5	2.43±0.15	15	17.87±0.35	102.52	1.96
		60	62.07±0.72	99.42	1.16
6	2.65±0.11	15	17.16±0.52	97.22	3.03
		60	62.93±0.72	100.45	1.14
7	2.48±0.07	15	17.05±0.44	97.54	2.58
		60	63.17±0.62	101.1	0.98
8	2.62±0.08	15	17.35±0.53	98.47	3.05
		60	61.32±0.54	97.92	0.88
9	2.23±0.11	15	17.68±0.37	102.02	2.09
		60	63.28±0.73	101.52	1.15
10	2.24±0.10	15	17.92±0.38	103.94	2.12
		60	63.97±0.74	102.78	1.16

REFERENCES

1. X. Hu, W. Wang and Y. Huang, *Talanta*, 2016, **154**, 409-415.
2. P. Choudhary, A. Kumar and V. Krishnan, *Chem. Eng. J.*, 2022, **431**, 133695.
3. R. Jalili, M. Dastborhan, S. Chenaghlou and A. Khataee, *J. Photochem. Photobiol., A*, 2020, **391**, 112370.
4. Z. Zhao, T. Lin, W. Liu, L. Hou, F. Ye and S. Zhao, *Spectrochim. Acta, Part A*, 2019, **219**, 240-247.
5. L. Su, W. Qin, H. Zhang, Z. U. Rahman, C. Ren, S. Ma and X. Chen, *Biosens. Bioelectron.*, 2015, **63**, 384-391.
6. H. Liu, Y. Hua, Y. Cai, L. Feng, S. Li and H. Wang, *Anal. Chim. Acta*, 2019, **1092**, 57-65.
7. X. Liu, X. Wang, Q. Han, C. Qi, C. Wang and R. Yang, *Talanta*, 2019, **203**, 227-234.
8. H. Yang, J. Wang, C. Yang, X. Zhao, S. Xie and Z. Ge, *J. Electrochem. Soc.*, 2018, **165**, H247.
9. W. Li, T. Li, S. Chen, D. Deng, Y. Ji and R. Li, *Sens. Actuators, B*, 2022, **355**, 131341.
10. J. Feng, X. Chen, X. Shi, W. Zheng, X. Zhang and H. Yang, *ECS J. Solid State Sci. Technol.*, 2022, **11**, 047001.
11. M. Masumoto, S. Ohta, M. Nakagawa, Y. Hiruta and D. Citterio, *Anal. Bioanal.Chem.*, 2022, **414**, 691–701.
12. U. Lad, G. M. Kale and R. Bryaskova, *J. Electrochem. Soc.*, 2014, **161**, B98.
13. Q. Yang, N. Li, Q. Li, S. Chen, H.-L. Wang and H. Yang, *Anal. Chim. Acta*, 2019, **1078**, 161-167.
14. L. Ai, L. Li, C. Zhang, J. Fu and J. Jiang, *Chemistry–A European Journal*, 2013, **19**, 15105-15108.
15. H.-M. Meng, X.-B. Zhang, C. Yang, H. Kuai, G.-J. Mao, L. Gong, W. Zhang, S. Feng and J. Chang, *Anal. Chem.*, 2016, **88**, 6057-6063.